ELSEVIER

Nuclear Physics A 641 (1998) 3–20

NUCLEAR PHYSICS A

Alpha spectroscopic factors for ^{6}Li, ^{7}Li, ^{9}Be and ^{12}C from the $(\vec{p}, p\alpha)$ reaction at 296 MeV

T. Yoshimura [a], A. Okihana [b], R.E. Warner [c], N.S. Chant [d], P.G. Roos [d], C. Samanta [e], S. Kakigi [a], N. Koori [f], M. Fujiwara [g], N. Matsuoka [g], K. Tamura [g], E. Kubo [b], K. Ushiro [b]

[a] *Institute for Chemical Research, Kyoto University, Uji, Kyoto 611, Japan*
[b] *Kyoto University of Education, Kyoto 612, Japan*
[c] *Department of Physics, Oberlin College, Oberlin, OH 44074, USA*
[d] *Department of Physics and Astronomy, University of Maryland, College Park, MD 20742, USA*
[e] *Saha Institute of Nuclear Physics, Calcutta 700064, India*
[f] *Department of Mathematical and Natural Sciences, Tokushima University, Tokushima 770, Japan*
[g] *Research Center for Nuclear Physics, Osaka University, Ibaraki, Osaka 567, Japan*

Received 28 May 1998; accepted 1 July 1998

Abstract

Three-body breakup cross sections and analyzing powers for the ^{6}Li, ^{7}Li, ^{9}Be and ^{12}C$(\vec{p}, p\alpha)$ reactions were measured at an incident energy of 296 MeV. Data were analyzed using the plane wave impulse approximation (PWIA) and the distorted wave impulse approximation (DWIA) and compared with previous studies. DWIA calculations reproduce shapes of projected spectra and analyzing power distributions fairly well with the exception of the ^{12}C$(\vec{p}, p\alpha)^{8}$Be reactions. Extracted spectroscopic factors for ^{6}Li, ^{9}Be and ^{12}C are larger than those found in the previous studies. In contrast, extracted spectroscopic factors for ^{7}Li agree with the previous work. This work suggests that the spectroscopic factor for ^{6}Li is ~ 0.8, independent of incident energies and reaction types. © 1998 Elsevier Science B.V.

Keywords: NUCLEAR REACTION ^{6}Li, ^{7}Li, ^{9}Be, ^{12}C$(\vec{p}, p\alpha)$, E = 296 MeV; measured $\sigma(\theta_p, \theta_\alpha, E_p)$, A_y; deduced alpha spectroscopic factor. Projected energy spectrum, analyzing power distribution, quasifree scattering, distorted wave impulse approximation.

1. Introduction

The cluster structure of light nuclei has been the subject of experimental and theoretical studies for many years. In particular, it appears that alpha cluster structures are often found in the ground-state wave functions of light nuclei, a result at least partially

PII S0375-9474(98)00432-1

due to the alpha particle's large binding energy and stability. The nuclear ground-state wave function may be projected onto a two-body cluster structure, in which the alpha particle is bound to the residual nucleus; the cluster structures are then characterized by spectroscopic factors and momentum distributions of the bound alpha particles relative to the residual core. Specifically, the spectroscopic factor is defined as the square of the normalization of the overlap amplitude between the target ground state and the residual system comprising the alpha particle and the core.

Historically, quasifree scattering (QFS) and transfer reactions have been used to investigate alpha cluster structures. If we ignore initial and final state interactions, the QFS process involves a projectile which interacts directly with an alpha particle without transferring any momentum to the core, i.e. the core remains a spectator. Spectator model descriptions such as the plane wave impulse approximation (PWIA) or distorted wave impulse approximation (DWIA) have had some success in describing cluster knockout reactions. Using these approaches spectroscopic factors, relative momentum distributions and spin observables of the elementary two-body processes can be extracted.

The nucleus ^{6}Li has the simplest alpha cluster structure in which an alpha particle is loosely bound to a deuteron or a p–n pair. The alpha cluster structure for this nucleus has been studied extensively. According to recent theoretical studies, the three-body $(\alpha + N + N)$ models predict spectroscopic factors S_α = 0.65–0.75 [1,2] for $\alpha + d$ clustering whereas microscopic and some resonating group theory models give larger values, S_α = 0.92–1.04 [3–7]. Experimentally, spectroscopic factors for ^{6}Li were extracted from the $(p, p\alpha)$ data at 100 MeV [8], the $(\alpha, 2\alpha)$ data at 77–120 MeV [9], the (p, pd) data at 120 [11] and 200 MeV [11], and the $(e, e'd)$ data at 480 MeV [13] using the DWIA theory. These experimental spectroscopic factors are plotted versus incident energy in Fig. 1. The spectroscopic factors are roughly divided into two groups; one near 0.8 extracted from deuteron knockout (p, pd) and $(e, e'd)$ reactions, and a second group between 0.4 and 0.6 extracted from alpha particle knockout. In addition, one notes a tendency for the spectroscopic factors to be larger at the higher incident energy. Theoretically, the spectroscopic factor should remain constant and independent

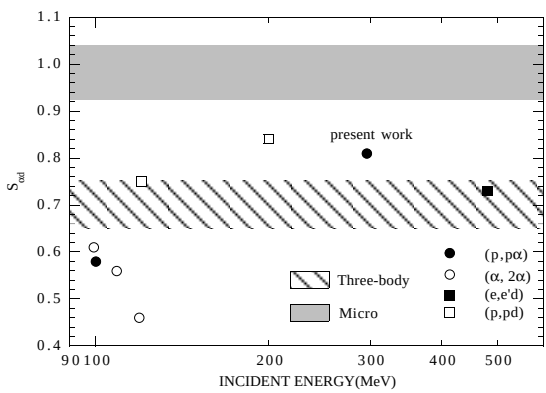

Fig. 1. Spectroscopic factors for ^{6}Li versus incident energy.

of incident energy or reaction type. The origin of the variation in the spectroscopic factors extracted from data is not yet clear. To investigate this problem, measurements at different incident energies are needed, especially at higher incident energies where the reaction mechanism description should be more reliable. For a measurement at around 300 MeV, which is easily accessible with the RCNP cyclotron, no data are currently available.

It is also well known that ^{7}Li, ^{9}Be and ^{12}C have large overlap with alpha cluster structures. For example, the ^{7}Li ground state has a large overlap with a bound two-cluster description consisting of an alpha particle and a triton. In this case, the relative angular momentum of the bound alpha cluster is $L = 1$, which leads to minimum in the QFS cross section at a kinematical condition where the residual triton has zero recoil momentum. According to Roos et al. [8], DWIA calculations reproduce reasonably the shapes of energy sharing distributions (differential cross sections plotted as a function of detected proton energy) in the $^{7}\mathrm{Li}(p, p\alpha)^{3}\mathrm{H}$ reaction at 100 MeV. However, these authors note that the predictions are slightly too broad, perhaps due to inaccuracies in the bound-state wave function or optical potentials. A value of $S_\alpha = 0.94$ for the ^{7}Li ground-state spectroscopic factor was obtained from the $(p, p\alpha)$ data at 100 MeV [8] which agrees with $S_\alpha = 1.12$ from simple LS coupling shell model calculations by Smirnov et al. [14]. However, the spectroscopic factor obtained from the $(\alpha, 2\alpha)$ data at 77–119 MeV by Warner et al. [15] is considerably larger than the $(p, p\alpha)$ value. In contrast, for ^{6}Li, the $(p, p\alpha)$ data at 100 MeV and the $(\alpha, 2\alpha)$ data at 77–119 MeV gave almost equal spectroscopic factors. Since it has been suggested that ^{7}Li may be more sensitive to distortions, it would be valuable to obtain data at higher incident energies.

The case of ^{9}Be is more complicated, since a bound alpha cluster can have a relative angular momentum of $L = 0$ or 2, and the residual ^{5}He is unbound. There are some studies of alpha cluster structures in ^{9}Be using QFS at incident energies near or above 100 MeV. For $(p, p\alpha)$ data at 100 MeV, Roos et al. [8] fitted DWIA calculations to data with the $L = 2$ and $L = 0$ spectroscopic factors equal and obtained values of S_α between 0.41 and 0.83 depending on angle. Nadasen et al. [16] obtained spectroscopic factors of $S_\alpha = 0.45$ for $L = 0$ and $S_\alpha = 0.55$ for $L = 2$. These extracted spectroscopic factors are in reasonably good agreement with shell model predictions by Kurath [21] of $S_\alpha = 0.56$ for both $L = 0$ and 2, but they are lower than the microscopic three-cluster model prediction by Arai et al. [22] of $S_\alpha = 0.84$ for $L = 0$. On the other hand, DWIA calculations did not reproduce the shapes of energy sharing distributions at forward angles in studies of the $(p, p\alpha)$ and $(\alpha, 2\alpha)$ reactions at 150–200 MeV [18,20,19]. In addition, analyzing power distributions do not agree with DWIA predictions except at proton scattering angles of $\theta_p = 70^\circ$ and 80° in the $(p, p\alpha)$ data at 150 MeV by Wang et al. [18]. These authors pointed out that other processes may well contribute, for example, multistep processes which do not have the same analyzing powers as QFS. Again, measurements at higher energies are desirable since those contributions may well be reduced.

Finally, for ^{12}C, there are a few studies of alpha cluster structures using QFS. Spec-

troscopic factors for the ground state transition of S_α = 0.35–0.81 for α+^{8}Be clustering were obtained from the $(p, p\alpha)$ data at 100 MeV [8]. The average of these values is in agreement with the shell model prediction of S_α = 0.56 [21] but there remain uncertainties due to large distortions as was pointed out by Nadasen et al. [20].

In view of these results and the concerns outlined above, we measured cross sections and analyzing power data for the ^{6}Li, ^{7}Li, ^{9}Be and ^{12}C$(\vec{p}, p\alpha)$ reactions at 296 MeV. It was hoped that the analyzing powers would be sensitive to contributions to these reactions from processes other than QFS.

2. Experiment

This experiment was carried out at the Research Center for Nuclear Physics (RCNP), Osaka University. A polarized proton beam was accelerated to 296 MeV by the RING cyclotron and transported to a 1.6 m diameter scattering chamber. The beam polarization was monitored by a polarimeter located approximately 36 m upstream from the center of the scattering chamber. The polarimeter consisted of a CH_2 target and four NaI(Tl) scintillation counters which counted scattered and recoil protons from the ^{1}H(p,p) reaction in the horizontal plane containing the beam. The polarization varied between 0.66 and 0.71. The targets were isotopically enriched ^{6}Li, ^{7}Li, ^{9}Be, and ^{12}C foils of thicknesses were 9.2, 9.3, 4.7 and 4.1 mg/cm^2, respectively. The targets were mounted in stainless steel frames and attached to a movable stainless steel ladder at the center of the scattering chamber.

Protons were detected using the large acceptance spectrograph(LAS) [23]. The LAS spectrograph consists of a magnetic quadrupole followed by a dipole (QD) with four vertical drift chambers (VDC's) and two trigger counters each consisting of three thin plastic scintillators. The LAS momentum acceptance is 30% and the nominal angular acceptance is 120 mrad horizontally and 200 mrad vertically. It is known that the effective solid angle is 20.4 msr [24]. However, if we restrict the horizontal acceptance to within $\pm$20 mrad of the central scattering angle then the effective solid angle falls to 7.2 msr [25]. The magnetic field of the LAS dipole magnet was set so that the central momentum corresponded to protons of 230 MeV kinetic energy. Momenta and scattering angles of the detected protons were determined from the VDC data and the magnetic parameters using a trace-back method in off-line analyses. Typical energy resolution of LAS was approximately 500 keV (FWHM) for ^{12}C elastic scattering peaks. Coincident alpha particles were detected by an E–ΔE counter telescope mounted in the horizontal plane on the opposite side of the incident beam from the spectrometer. The telescope consisted of a 150 μm Si-SSD surface barrier ΔE detector followed by a 5 mm Si-SSD lithium drift detector. The telescope solid angle of 2.26 msr was defined by a copper collimator with a hole of 11 mm diameter. The detection angle pairs are listed in Table 1.

The LAS VDCs signals were processed with a LeCroy PCOS III system. Trigger signals were generated when the two LAS trigger counters fired in coincidence. If the SSD telescope also detected a particle in coincidence with the LAS trigger, the data were

Table 1
Angle pairs

Reaction	θ_p/θ_α (deg)
^{6}Li$(p,p\alpha)^{2}$H	45.0/60.7
	55.0/54.7
^{7}Li$(p,p\alpha)^{3}$H	45.0/60.5
	55.0/54.6
^{9}Be$(p,p\alpha)^{5}$He	35.0/66.6
^{12}C$(p,p\alpha)^{8}$Be	35.0/65.8
	45.0/59.8

recorded as a coincident event. We also recorded a prescaled fraction of the LAS triggers as singles events. The SSD, VDC and time data were digitized in CAMAC modules and recorded on a DEC VAX computer using the ICHIHARA-Q data acquisition software.

To determine the integrated incident charge, a Faraday cup was temporarily mounted in the scattering chamber and used to obtain the ratio of the integrated charge to the counts recorded by the polarimeter. Using this normalization, we were able to obtain the integrated charge for each run from the polarimeter counts. The off-line analyses were done using the QPAW system with the AlphaServer 2100 4/200 computer at the RCNP.

3. Results

In Fig. 2 we present coincident energy maps for the ^{6}Li, ^{7}Li$(p,p\alpha)$ reactions at $\theta_p = 45^\circ$ and ^{9}Be, ^{12}C$(p,p\alpha)$ reactions at $\theta_p = 35^\circ$. Solid curves and dashed curves show kinematic loci for the $(p,p\alpha)$ and $(p,p^{3}\mathrm{He})$ breakup reactions leading to the ground states of the corresponding residual nuclei. In the figures, enhanced yields are seen around the loci for the $(p,p\alpha)$ reactions leading to the ground states of the various residual nuclei thus confirming the dominance of the three-body breakup process. Since alpha particles could not be separated completely from ^{3}He particles in the particle identification spectra computed from the E–ΔE counter telescope data, some yield for the $(p,p^{3}\mathrm{He})$ reaction may be included in each continuum region. However, due to large differences in Q-value, these yields are well separated from the ground-state $(p,p\alpha)$ loci and any resultant contamination of the ground-state $(p,p\alpha)$ yields is negligible.

For the ^{9}Be$(p,p\alpha)$ ground-state transition the residual nucleus is ^{5}He whose (unbound) ground state is composed of an α+n system at a relative energy of 0.9 MeV with a width of 0.6 MeV [42]. Similarly, for the ^{12}C$(p,p\alpha)$ ground-state reaction the residual nucleus is ^{8}Be, whose ground state is an unbound $\alpha+\alpha$ system at relative energy of 0.09 MeV and with a width of 6.8 eV [42]. Thus, in principle, the yields for these reactions may include four-body and higher phase-space contributions. In order to estimate these phase-space contributions to the ground-state transition, we calculated only four-body phase-space distributions. Higher-order phase-space terms contribute only at much larger values of the missing mass. Fig. 3 shows missing mass spectra for the

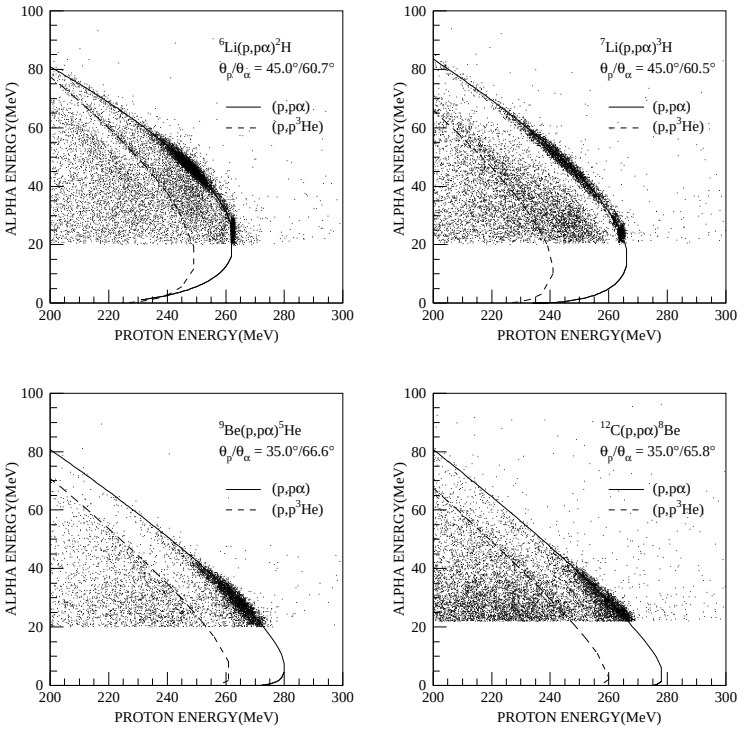

Fig. 2. Coincident energy maps for the ^{6}Li, ^{7}Li$(p,p\alpha)$ reactions at θ_p = 45° and the ^{9}Be, ^{12}C$(p,p\alpha)$ reactions at θ_p = 35°. Solid curves and dashed curves show kinematic loci for the three-body $(p,p\alpha)$ and $(p,p^{3}\mathrm{He})$ breakup reactions, respectively.

^{9}Be$(p,p\alpha)\alpha n$ and the ^{12}C$(p,p\alpha)\alpha\alpha$ reactions. The solid curves show arbitrarily normalized four-body phase-space distributions. Sharp peaks are seen at missing mass energies for each residual nucleus ground state. Small peaks around 19 MeV correspond to contamination yields from the three-body $(p,p^{3}\mathrm{He})$ breakup reaction. Roos et al. [8] observe a peak for the first excited state $(2+)$ of ^{8}Be in the ^{12}C$(p,p\alpha)^{8}$Be reaction at 100 MeV. Unfortunately, our missing mass resolution prevents separation of this state from the ^{8}Be ground state. These estimations indicate that the four-body phase-space contributions to the three-body breakup yields are below $\sim$ 3% for the ^{9}Be$(p,p\alpha)^{5}$He reaction and below $\sim$ 8% for ^{12}C$(p,p\alpha)^{8}$Be reactions. The ground-state cross sections were then obtained by projecting the remaining yield corresponding to $E_{\mathrm{miss}} \leqslant 5$ MeV onto the proton energy axis.

The projected spectra and analyzing power distributions are presented in Figs. 4–6, where the presented errors are statistical errors only. Absolute errors in the cross section are estimated to be less than 10%. Arrows show points satisfying the kinematic QFS condition for which the residual nuclei have zero recoil momentum. For the ^{6}Li$(p,p\alpha)^{2}$H reaction in which the struck alpha particle is bound to the residual deuteron with relative angular momentum L = 0, the cross section reaches a maximum at the QFS point as expected. In addition, at a higher proton energy, peaks corresponding to sequential de-

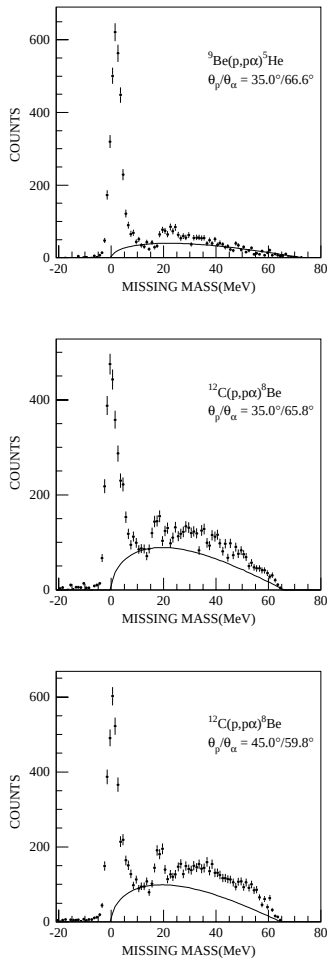

Fig. 3. Missing mass spectra and normalized four-body phase-space calculations for the ^{9}Be$(p,p\alpha)\alpha$n and the ^{12}C$(p,p\alpha)\alpha\alpha$ reactions. Solid curves show the four-body phase space. Small peaks around 19 MeV correspond to yields from the three-body $(p,p^{3}$He) breakup reaction.

cays through low-lying excited states of ^{6}Li are visible. In the case of the ^{7}Li$(p,p\alpha)^{3}$H reaction, the alpha particle and residual triton in ^{7}Li are bound with relative angular momentum $L = 1$. As a result, a minimum is expected at the QFS point. In fact, the data are fairly flat at the QFS point for $\theta_p/\theta_\alpha = 45.0°/60.5°$ and a exhibit a slight dip for $\theta_p/\theta_\alpha = 55.0°/54.6°$. In addition, as noted for ^{6}Li$(p,p\alpha)^{2}$H, sequential decay peaks are seen at higher proton energies. For the ^{9}Be$(p,p\alpha)^{5}$He reaction, a maximum is observed at the QFS point presumably due to the $L = 0$ contribution to the reaction. Contributions from sequential decays are not clearly identified. However, since ^{9}Be has known excited states up to about 20 MeV, there may well be some sequential contributions at energies above the QFS point. For the ^{12}C$(p,p\alpha)^{8}$Be$(0+)$ reaction, the relative angular momentum is again $L = 0$ as noted for ^{6}Li and ^{9}Be. However, a QFS peak is not clearly visible.

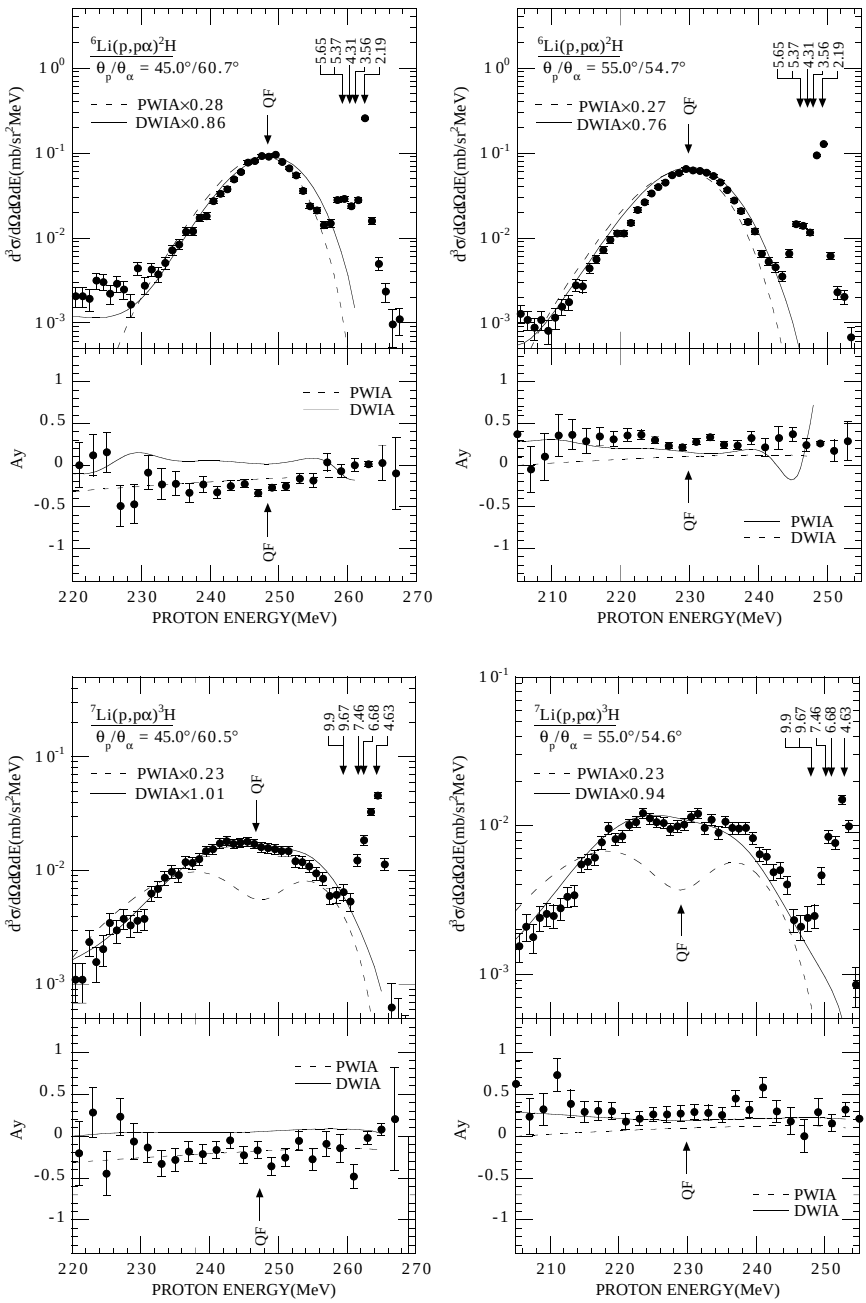

Fig. 4. Cross sections and polarization analyzing power distributions projected onto the proton energy axis for the ^{6}Li$(p,p\alpha)^2$H(g.s.) and ^{7}Li$(p,p\alpha)^3$H(g.s.) reactions. Solid curves and dashed curves represent DWIA and PWIA calculations, respectively. Arrows labeled "QF" indicate points of zero recoil momentum. Some arrows labeled numbers mark expected locations of sequential decays from the ^{6}Li or ^{7}Li excited states.

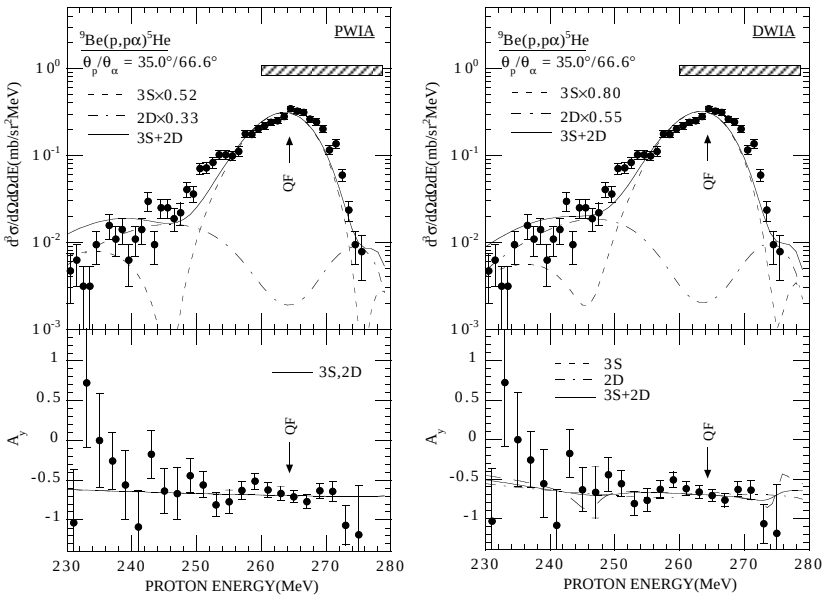

Fig. 5. Cross sections and polarization analyzing power distributions projected onto the proton energy axis for the ^{9}Be$(p, p\alpha)^5$He(g.s.) reaction. Dashed and dot-dashed curves show DWIA (or PWIA) calculations for $L = 0$ and $L = 2$ components, respectively. Solid curves show their sum normalized. Labeled arrows indicate points of zero recoil momentum. Hatched rectangles mark expected locations of sequential decays from the ^{9}Be excited states.

We conjecture that this peak is perhaps obscured by large contributions from sequential decays. In addition, we note that an admixture of yield from the ^{12}C$(p, p\alpha)^8$Be$(2+)$ reaction corresponding to $\alpha+^8$Be$(2+)$ clustering with $L = 2$ would influence the shapes of the projected spectra.

The polarization analyzing powers are fairly constant around the QFS point for all targets, with the exception of ^{12}C which does show some modest variation. The PWIA curve, shown in each figure, is identically equal to the analyzing powers for free $p + \alpha$ scattering at appropriate kinematics. The observed consistency of our data with this very simple prediction for the analyzing power strongly supports our description of the reaction mechanism as a simple quasi-free scattering from alpha cluster configurations in the target nuclei wave functions.

4. DWIA/PWIA analyses

In this experiment, both analyzing powers and differential cross sections were measured for the $(p, p\alpha)$ reaction. Since the analyzing powers depend upon interference effects or small differences between the reaction amplitudes, one can anticipate greater sensitivity to details of the reaction mechanisms than in the differential cross section data. In particular, the analyzing power data may provide some indication as to the importance of contributions from processes other than QFS. For analyzing powers in

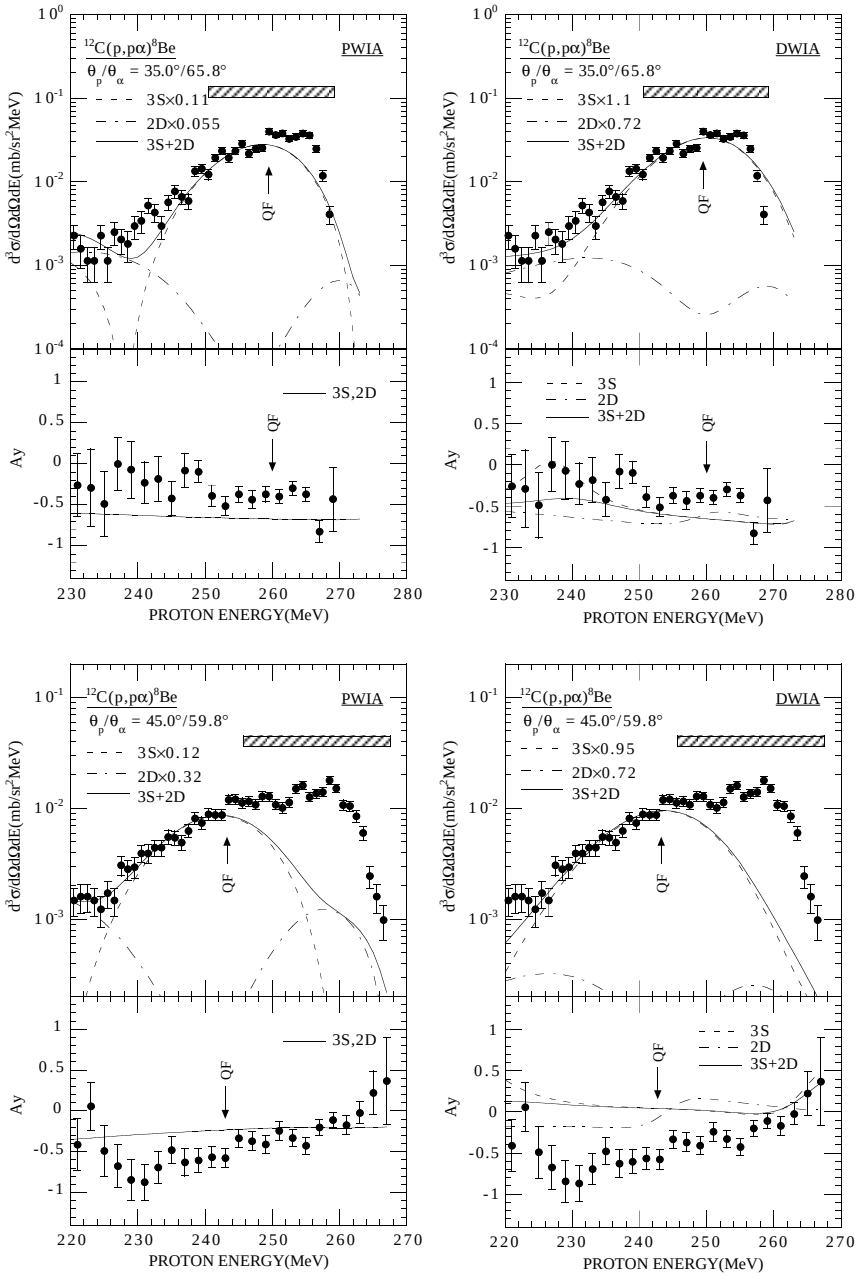

Fig. 6. Cross sections and polarization analyzing power distributions projected onto the proton energy axis for the $^{12}C(p, p\alpha)^{8}Be$ reaction. Dashed and dot-dashed curves show DWIA (or PWIA) calculations for $L = 0$ and $L = 2$ components, respectively. Solid curves show their sum normalized. Labeled arrows indicate points of zero recoil momentum. Hatched rectangles mark expected locations of sequential decays from the ^{12}C excited states.

$(p, p\alpha)$ reactions, measurements have been reported only for the ^{9}Be$(p, p\alpha)^{5}$He reaction at 150 MeV [18] and the ^{6}Li$(p, p\alpha)^{2}$H reaction at 40 MeV [43]. It is also of note that spin observables such as analyzing powers cannot be treated realistically by previous DWIA calculations which did not include spin–orbit terms in the optical potentials. Fortunately, this restriction has been eliminated in the calculations by Chant et al. [40] who extended the previous DWIA theory to include spin–orbit distortions. Following the notation of Chant et al., we consider the $A(a, cd)B$ reaction in which a projectile a interacts with a cluster b in the target A leading to three particles c, d and B in the final state. If we restrict discussion to the $(p, p\alpha)$ reaction, we have $a = c$ and $b = d$. Moreover, particles b, d are spin-less. In this case, the differential cross section of the reaction can be written

$$\frac{d^3\sigma}{d\Omega_c d\Omega_d dE} = S_\alpha \times KF \times \sum_{\substack{\rho_c' \\ L\Lambda}} \left| \sum_{\rho_a \sigma_a \sigma_c \sigma_c'} D^{S_a}_{\rho_a \rho_a'} \left(R_{ap}\right) D^{S_a^*}_{\sigma_c \sigma_c'} \left(R_{ac}\right) T^{L\Lambda}_{\substack{\sigma_a \sigma_c' \\ \rho_a \rho_c'}} \langle \sigma_c | \, t \, | \sigma_a \rangle \right|^2, \tag{1}$$

where S_α is a cluster spectroscopic factor, KF is a kinematic factor which includes the phase space for the three-body breakup reaction and the D's are rotation matrices. The quantity $\langle \sigma_c | \, t \, | \sigma_a \rangle$ is the t matrix element for the elementary two-body scattering process $a + b \rightarrow c + d$. The quantity $T^{L\Lambda}_{\substack{\sigma_a \sigma_c' \\ \rho_a \rho_c'}}$ is defined by

$$T^{L\Lambda}_{\substack{\sigma_a \sigma_c' \\ \rho_a \rho_c'}} = (2L+1)^{-1/2} \int \chi^{(-)*}_{\sigma_c' \rho_c'} (r) \, \chi^{(-)*}_{\alpha} (r) \, \phi_{L\Lambda} (r) \, \chi^{(+)}_{\sigma_a' \rho_a} (\gamma r) \, dr, \tag{2}$$

where the χ's are incoming or outgoing distorted waves and $\phi_{L\Lambda}(r)$ is a "bound-state wave function" of the cluster b. See Ref. [40] for more details about Eqs. (1), (2). More properly, the bound-state wave function is the projection of the target wave function on the product of alpha cluster and residual nucleus wave functions.

In both PWIA and DWIA calculations with spin–orbit potentials omitted, the half off-shell cross section for the two-body $a + b \rightarrow c + d$ process appears as a multiplicative factor. Frequently, it is simply approximated by the on-shell cross section at a nearby kinematics point. However, it is evident from Eq. (1) that the corresponding t-matrix enters in a coherent sum and the above approximation is no longer appropriate. In our DWIA calculations, carried out using the computer code THREEDEE by Chant et al. [29], the t matrix elements of the elementary $p + \alpha$ process were calculated from an optical potential fitted to angular distribution data. The potential is a Woods–Saxon type including absorption and spin–orbit terms. Differential cross sections at 300 MeV were obtained by interpolating cross sections obtained at energies between 200 and 500 MeV [27]. Analyzing power data at 300 MeV were taken from Ref. [26]. The interpolated and measured data are presented in Fig. 7. Clearly, the interpolation and the fit seem to be reasonable. The optical parameters were obtained using the computer code MAGALI by Raynal. Angular distributions from the resultant optical potential are shown as solid curves in Fig. 7. The parameters are listed in Table 2.

Table 2
Optical potential parameters

System	θ_p	V	r	a	W	W_s	r_w	a_w	V_{ls}	W_{ls}	r_{ls}	a_{ls}	r_c	Ref.
$p+^{6}$Li	All													[30]
$\alpha + d$	45.0	85.5	1.32	0.620	0.0	1.70	3.23	0.650					1.64	[38]
	55.0	78.3	1.32	0.620	0.0	2.30	3.23	0.650					1.64	[38]
$p + d$	All	38.5	0.989	0.285	92.0	0.0	0.535	0.0640					1.60	[39]
$p+^{7}$Li	All													[30]
$\alpha + t$	All	70.4	2.00	0.543	1.76	0.0	2.54	2.21					1.20	[36]
$p + t$	45.0	6.39	1.25	0.275	2.78	0.0	1.74	0.0185	6.27	−4.51	0.540	0.491	1.30	[32]
	55.0	4.10	1.17	0.243	3.27	0.0	1.74	0.0469	7.21	−4.68	0.546	0.496	1.30	[32]
$p+^{9}$Be	35.0													[30]
$\alpha+^{5}$He	35.0	107	1.14	0.700	1.0		1.14	0.700					1.14	[20]
$p+^{5}$He	35.0	4.20	1.42	0.0162	23.3	0.0	1.40	0.433	6.90	−6.88	0.822	0.295	1.36	[27,26]
$p+^{12}$C	All													[30]
$\alpha+^{8}$Be	All	55.3	1.77	0.613	0.0	22.6	1.45	0.470					1.48	[34]
$p+^{8}$Be	All	5.94	1.57	0.387	47.6	0.0	0.564	0.675	1.94	−1.35	1.14	0.599	1.12	[31]
$p + \alpha$	All	5.44	1.50	0.115	27.2	0.0	1.17	0.582	4.45	−6.77	0.826	0.314	1.36	

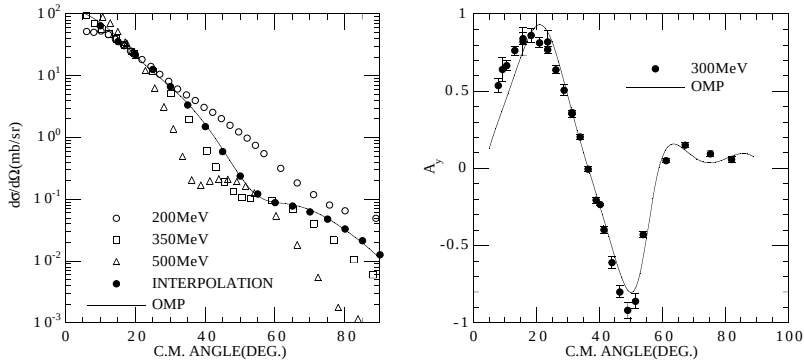

Fig. 7. (a) Comparison of the interpolated and experimental cross sections for elastic $p+\alpha$ scattering. Filled circles, open circles, squares and triangles represent the interpolated cross sections at 296 MeV and the experimental cross sections at the energies 200, 350 and 500 MeV [27], respectively. The solid curve is the angular distribution calculated from the fitted optical potential. (b) The angular distribution of measured analyzing powers for the elastic $p+\alpha$ scattering at 300 MeV [26]. The solid curve is the optical model prediction.

The projectile and ejectile distorted waves were generated using appropriate optical potentials. In principle, the interaction of the projectile with the ejected cluster is taken into account to all orders via the two-body t-matrix for the elementary $p+\alpha$ interaction. In order to take this into account in an approximate fashion, phenomenological Dirac optical potentials for the incident proton by Cooper et al. [30] were reduced in strength. Specifically, the nuclear potential depths were multiplied by the mass ratio of the core to the target, while the Coulomb potential depths were reduced by the corresponding charge ratio. For the outgoing particles, conventional Woods–Saxon type optical potentials were used. These potentials were obtained from fitting experimental elastic scattering data or, in some cases, interpolations of experimental data. For $p+^5$He and $\alpha+^5$He scattering, potential depths were increased by a factor of $5/4$ from those obtained from fits to $p+\alpha$ and $\alpha+\alpha$ data, respectively. Similarly, $p+^9$Be and $\alpha+^9$Be potentials were reduced by a factor of $8/9$ in order to calculate distorted waves for $p+^8$Be and $\alpha+^8$Be, respectively. The potential parameters used are listed in Table 2.

For the bound-state wave functions, we used the same Woods–Saxon potentials selected by Roos et al. [8] for DWIA/PWIA analyses of ^{6}Li, ^{7}Li, ^{9}Be and ^{12}C$(p,p\alpha)$ reactions at 100 MeV. This choice should serve to simplify comparisons with this earlier work. The orbital angular momenta of these wave functions are restricted by conservation of angular momentum and parity. The allowed angular momenta are $L=0$ and 2 for ^{6}Li, $L=1$ for ^{7}Li, $L=0$ and 2 for ^{9}Be and $L=0$ for ^{12}C. For ^{6}Li, however, only the $L=0$ term was used since it has been shown that the $L=2$ component of the wave function is very small and can be neglected [41,1]. In order to estimate contributions from $\alpha+^8$Be$(2+)$ clustering on ^{12}C as mentioned above, we carried out calculations for the clustering with $L=2$ too. The potential parameters are listed in Table 3.

Finally, we carried out corrections for the large vertical acceptance of the LAS spectrometer. The LAS has a vertical acceptance of -100 to $+100$ mrad as mentioned in

Table 3
Spins of target and clusters and parameters of bound-state functions

$J_A^{\pi_A}$	$J_b^{\pi_b}$	$J_B^{\pi_B}$	N, L	V	r	a	r_c	Ref.
^{6}Li(1^+)	$\alpha(0^+)$	d(1^+)	2,0	77.0	1.47	0.71	1.47	[8]
^{7}Li($3/2^-$)	$\alpha(0^+)$	t($1/2^+$)	2,1	91.9	1.43	0.72	1.43	[8]
^{9}Be($3/2^-$)	$\alpha(0^+)$	^{5}He($3/2^-$)	3,0 and 2,2	89.0	1.35	0.73	1.35	[8]
^{12}C(0^+)	$\alpha(0^+)$	^{8}Be(0^+)	3,0	89.9	1.23	0.75	1.23	[8]
^{12}C(0^+)	$\alpha(0^+)$	^{8}Be(2^+)	2,2	99.7	1.23	0.75	1.23	[8]

Section 2. At QF points, as the maximum out-of-plane acceptance angle ϕ increases from 0°, non-zero momentum components of the (distorted) momentum distributions contribute. Thus, it is expected that the projected spectra will become broader with lower maxima, and the expected minima in the case of $L = 1$ will become less apparent or even vanish completely. As a result, if appropriate corrections for the large vertical acceptance of the LAS are not made, reduced values of spectroscopic factors will be extracted. For the corrections, DWIA and PWIA calculations were performed at out-of-plane angles ϕ from -100 to 100 mrad in 20 mrad steps. These predictions were then summed in proportion to weights calculated using the Monte Carlo method.

5. DWIA/PWIA results and discussion

DWIA and PWIA calculations were carried out using both initial and final energy prescriptions. However, there were only small differences in the predictions obtained using these two approximations. We therefore present only results using the final energy prescription. The small size of these differences also suggests that our use of an on-shell approximation may be reasonable at 296 MeV.

Fig. 4 shows DWIA and PWIA calculations for the ^{6}Li$(p, p\alpha)^2$H and ^{7}Li$(p, p\alpha)^3$H reactions, where solid and dashed curves indicate DWIA and PWIA predictions, respectively. For the ^{6}Li$(p, p\alpha)^2$H reaction, both calculations reproduce the shapes of the projected spectra very well. For the ^{7}Li$(p, p\alpha)^3$H reaction, the minima near QF points in the PWIA calculations do not reproduce the shapes of the projected spectra. This behavior was also observed in the $(p, p\alpha)$ data at 100 MeV [8]. The introduction of distortion effects as well as appropriate averaging over the LAS solid angle in the DWIA calculations cause the PWIA minimum to be filled in. As a result, the DWIA predictions reproduce the experimental shapes well although DWIA predictions for ^{7}Li in the $(p, p\alpha)$ data at 100 MeV [8] and the $(\alpha, 2\alpha)$ data at 77–119 MeV [9] were found to be broader than the experimental distributions. For the ^{6}Li$(p, p\alpha)^2$H and ^{7}Li$(p, p\alpha)^3$H reactions, analyzing power distributions are reproduced reasonably well by both DWIA and PWIA theories.

For the ^{9}Be$(p, p\alpha)^5$He reaction, DWIA and PWIA calculations for the $L = 0$ and $L = 2$ components were carried out and are presented in Fig. 5, where dashed and dot-dashed curves show calculations for $L = 0$ and $L = 2$ components, respectively.

Table 4
Spectroscopic factors

Reaction	θ_p/θ_α(deg.)	S_α
^{6}Li$(p,p\alpha)^2$H	45.0/60.7	0.86
	55.0/54.7	0.76
^{7}Li$(p,p\alpha)^3$H	45.0/60.5	1.01
	55.0/54.6	0.94
^{9}Be$(p,p\alpha)^5$He	35.0/66.6	0.80
^{12}C$(p,p\alpha)^8$Be	35.0/65.8	1.1
	45.0/59.8	0.95

The predictions were normalized at proton energies below the QF point using the method of least squares, with the spectroscopic factor for the $L = 2$ component fixed at the value of 0.55 extracted from the non-coplanar $(p,p\alpha)$ experiment by Nadasen et al. [16]. Solid curves show the sum which is somewhat narrower than the experimental distribution. The same trend was observed in the $(p,p\alpha)$ data at 150 MeV [18] and 200 MeV [20], and the $(\alpha,2\alpha)$ data at 197 MeV [19]. At higher detected proton energies, the discrepancies can be understood as contributions from sequential decays. At lower detected proton energies, on the other hand, it has been suggested there might be contributions from multistep processes [18]. However, the analyzing power distribution for the ^{9}Be$(p,p\alpha)^5$He reaction is almost flat and agrees fairly well with both DWIA and PWIA predictions. In view of this result, we might argue that the reaction is largely a quasi-free process and there can be little contribution from multistep processes.

Fig. 6 presents DWIA and PWIA calculations for the sum of the $L = 0$ $\alpha+^8$Be$(0+)$ transition and the $L = 2$ $\alpha+^8$Be$(2+)$ transition shown as dashed and dot-dashed curves, respectively. Normalizations were performed with the spectroscopic factor for the $L = 2$ transition fixed at the value of 0.72 predicted by Kurath [21]. Solid curves show their sum normalized. DWIA and PWIA calculations reproduce the shapes of the projected spectra only at proton energies below the QF points due to large yields from sequential decays. Analyzing power distributions differ significantly from the DWIA and PWIA predictions suggesting that, for the ^{12}C$(p,p\alpha)^8$Be reaction even at 296 MeV, there are large contributions from processes other than QFS.

Extracted spectroscopic factors are listed in Table 4. For ^{6}Li, values of $S_\alpha = 0.86$ and 0.76 are obtained. These values are larger than those extracted from the $(p,p\alpha)$ data at 100 MeV [8] but agree with those extracted from the (p,pd) data at 120 and 200 MeV [11] and the $(e,e'd)$ data at 480 MeV [13]. Referring to Fig. 1, we see that our results are somewhat larger than the group of spectroscopic factors at lower energies with values between 0.4 and 0.6. Rather, they lie midway between the three-body model predictions $S_\alpha \sim 0.7$ and the microscopic model predictions $S_\alpha \sim 0.9$. This result suggests that we may have reached a constant value for the spectroscopic factor for ^{6}Li of $S_\alpha \sim 0.8$ and that, at higher energies, extracted spectroscopic factors for ^{6}Li should be largely independent of incident energy and reaction type.

For ^{7}Li, values of S_α = 1.01 and 0.94 are obtained. These agree with both the shell model prediction [14] and with spectroscopic factors extracted from the $(p, p\alpha)$ data at 100 MeV [8]. This result is unexpected in view of the disagreement with the result of the 100 MeV experiment on ^{6}Li. In the case of ^{9}Be, the extracted spectroscopic factor for $L = 0$ is $S_\alpha = 0.80$. This value is somewhat larger than both the shell model prediction $S_\alpha = 0.56$ [21] and the spectroscopic factors $S_\alpha = 0.38$–0.63 obtained previously [8,16,18,20,17,19]. Rather, the value agrees best with the microscopic three-cluster model prediction of $S_\alpha = 0.84$ [22]. The value chosen for $L = 2$ of 0.55 [16] appears to be reasonable since the normalized calculations successfully reproduce shapes of the projected spectra at low proton energy, we note that equal values for the spectroscopic factors for both $L = 0$ and 2 are predicted by Kurath [21]. For $\alpha+^{8}$Be$(0+)$ clustering on ^{12}C, the extracted spectroscopic factors are $S_\alpha = 1.1$ and 0.95, larger than both the shell model prediction [21] and the values of $S_\alpha = 0.56$ and $S_\alpha = 0.59$ extracted from the $(p, p\alpha)$ data at 100 MeV [8]. Finally, it is noted that, although the spectroscopic factors for the ^{6}Li, ^{9}Be$(L = 0)$ and ^{12}C transitions, which (in principle) peak at the QF points, are larger than those obtained in previous studies, the spectroscopic factors for ^{7}Li which exhibit minima at the QF points agree with previous results. Taking these results at face value, this suggests that the $L = 0$ cluster-core configurations may be more susceptible than are $L > 0$ configurations to enhancement from small residual interaction terms not normally included in simple shell model calculations.

In conclusion, we have measured cross sections and analyzing powers of the ^{6}Li, ^{7}Li, ^{9}Be and ^{12}C$(\vec{p}, p\alpha)$ reactions at 296 MeV and compared the results with DWIA and PWIA calculations. The DWIA calculations reproduce the shapes of the projected spectra and analyzing power distributions fairly well with the exception of the ^{12}C$(\vec{p}, p\alpha)^{8}$Be reactions. The extracted spectroscopic factors for ^{6}Li, ^{9}Be$(L = 0)$ and ^{12}C are larger than those found in previous studies. In contrast, extracted spectroscopic factors for ^{7}Li agree with previous work. Our 296 MeV incident energy measurement of the spectroscopic factor for ^{6}Li suggests that we may have reached a constant, energy independent value.

Acknowledgements

This work was funded in part by the Japan Society for the Promotion of Science (JSPS) and by the U.S.A. National Science Foundation under grants PHY-9423659 and PHY-9513924. We thank the staff of the Research Center for Nuclear Physics of Osaka University for their excellent support during this experiment, which was performed at the RCNP under Program Number R04.

References

[1] D.R. Lehman and Mamta Rajan, Phys. Rev. C 25 (1982) 2743.
[2] V.I. Kukulin, V.M. Krasnopol'sky, V.T. Voronchev and P.B. Szonov, Nucl. Phys. A 417 (1984) 128.
[3] R. Beck, F. Dickmann and R.G. Lovas, Nucl. Phys. A 446 (1985) 703.

[4] R.G. Lovas, A.T. Kruppa, R. Beck and F. Dickmann, Nucl. Phys. A 474 (1987) 451.
[5] K. Varga, Phys. Rev. C 43 (1991) 1201.
[6] A. Csótó, Phys. Rev. C 46 (1992) 576.
[7] H. Walliser and Y.C. Tang, Phys. Lett. B 135 (1984) 344.
[8] P.G. Roos, N.S. Chant, A.A. Cowley, D.A. Goldberg, H.D. Holmgren and R. Woody, III, Phys. Rev. C 15 (1977) 57.
[9] A. Okihana, T. Konishi, R.E. Warner, D. Francis, M. Fujiwara, N. Matsuoka, K. Fukunaga, S. Kakigi, T. Hayashi, J. Kasagi, N. Koori, M. Tosaki and M. Greenfield, Nucl. Phys. A 549 (1992) 1.
[10] W. Dollhopf, C.F. Perdrisat, P. Kitching and W.C. Olsen, Phys. Lett. B 58 (1975) 425.
[11] R.E. Warner, J-Q, Yang, D.L. Friesel, P. Schwandt, G. Caskey, A. Galonsky, B. Remington, A. Nadasen, N.S. Chant, F. Khazaie and C. Wang, Nucl. Phys. A 443 (1985) 64.
[12] D. Albrecht, M. Csatlós, J. Erö, Z. Fodor, I. Hernyes, Hongsung Mu, B.A. Khomenko, N.N. Khovanskij, P. Koncz, Z.V. Krumstein, Yu.P. Merekov, V.I. Petrukhin, Z. Seres and L. Végh, Nucl. Phys. A 338 (1980) 477.
[13] R. Ent, B.L. Berman, H.P. Blok, J.F.J. van den Brand, W.J. Briscoe, M.N. Harakeh, E. Jans, P.D. Kunz and L. Lapikás, Nucl. Phys. A 578 (1994) 93.
[14] Yu.F. Smirnov and D. Chlebowska, Nucl. Phys. 26 (1961) 306.
[15] R.E. Warner, A. Okihana, M. Fujiwara, N. Matsuoka, S. Kakigi, S. Hayashi, K. Fukunaga, J. Kasagi and M. Tosaki, Phys. Rev. C 45 (1992) 2328.
[16] A. Nadasen, N.S. Chant, P.G. Roos, T.A. Carey, R. Cowen, C. Samanta and J. Wesick, Phys. Rev. C 22 (1980) 1394.
[17] C.W. Wang, N.S. Chant, P.G. Roos, A. Nadasen and T.A. Carey, Phys. Rev. C 21 (1980) 1705.
[18] C.W. Wang, P.G. Roos, N.S. Chant, G. Ciangaru, F. Khazaie, D.J. Mack, A. Nadasen, S.J. Mills, R.E. Warner, E. Norbeck, F.D. Becchetti, J.W. Janecke and P.M. Lister, Phys. Rev. C 31 (1985) 1662.
[19] A.A. Cowley, G.F. Steyn, S.V. Förtsch, J.J. Lawrie, J.V. Pilcher, F.D. Smit and D.M. Whittal, Phys. Rev. C 50 (1994) 2449.
[20] A. Nadasen, P.G. Roos, N.S. Chant, C.C. Chang, G. Ciangaru, H.F. Breuer, J. Wesick and E. Norbeck, Phys. Rev. C 40 (1989) 1130.
[21] D. Kurath, Phys. Rev. C 7 (1973) 1390.
[22] K. Arai, Y. Ogawa, Y. Suzuki and K. Varga, Phys. Rev. C 54 (1996) 132.
[23] N. Matsuoka, T. Noro, K. Sagara, S. Morinobu, A. Okihana and K. Hatanaka, RCNP Ann. Rep. 1990 (1991) 235.
[24] A. Okihana, N. Matsuoka, T. Noro and M. Yoshimura, RCNP Ann. Rep. 1994 (1995) 150.
[25] K. Ushiro, private communication.
[26] M. Yoshimura, S. Yamamura, S. Kuwamoto, M. Nakamura, Y. Sakemi, H. Akimune, A. Yamagoshi, M. Yosoi, H. Togawa and T. Noro, RCNP Ann. Rep. 1992 (1993) 48;
M. Yoshimura, private communication.
[27] G.A. Moss, L.G. Greeniaus, J.M. Cameron, D.A. Hutcheon, R.L. Liljestrand, C.A. Miller, G. Roy, B.K.S. Koene, W.T.H. van Ores, A.W. Stetz, A. Willis and N. Willis, Phys. Rev. C 21 (1980) 1932.
[28] H. Sakaguchi, A. Yamagoshi, M. Yosoi, A. Tamii, S. Toyama, H. Akimune, I. Daito, T. Inomata, K. Hosono, M. Fujiwara and T. Noro, RCNP Ann. Rep. 1993 (1994) 4.
[29] N.S. Chant, private communication.
[30] E.D. Cooper, S. Hama, B.C. Clark and R.L. Mercer, Phys. Rev. C 47 (1993) 297.
[31] G. Roy, H.S. Sherif, E.D. Cooper, L.G. Greeniaus, G.A. Moss, J. Soukup, G.M. Stinson, R. Abegg, D.P. Gurd, D.A. Hutcheon, R. Liljestrand and C.A. Miller, Nucl. Phys. A 442 (1985) 686.
[32] D.K. Hasell, A. Bracco, H.P. Gubler, W.P. Lee, W.T.H. van Oers, R. Abegg, D.A. Hutcheon, C.A. Miller, J.M. Cameron, L.G. Greeniaus, G.A. Moss, M.B. Epstein and D.J. Margaziotis, Phys. Rev. C 34 (1986) 236.
[33] K. Fukunaga, H. Nakamura and N. Fujiwara, J. Phys. Soc. Japan 23 (1967) 911.
[34] R.G. Summers-Gill, Phys. Rev. 109 (1958) 1591.
[35] O.K. Gorpinich, V.I. Konfederatenko, V.V. Ostashko, O.M. Povoroznik, A.T. Rudchik and B.G. Struzhko, Bull. Russ. Acad. Sci. Phys. 56 (1992) 439.
[36] J.S. Vincent and E.T. Boschitz, Nucl. Phys. A 143 (1970) 121.
[37] A.M. Yasnogorodsky, V.V. Ostashko, V.N. Urin and A.N. Nenakhov, J. Phys. Soc. Japan 55 (1986) Suppl. 892.
[38] B. Jenny, W. Grüebler, V. König, P.A. Schmelzbach and C. Schweizer, Nucl. Phys. A 397 (1983) 61.

[39] R.D. Schamberger, Phys. Rev. 85 (1952) 424.
[40] N.S. Chant and P.G. Roos, Phys. Rev. C 27 (1983) 1060.
[41] J.W. Watson, H.G. Pugh, P.G. Roos, D.A. Goldberg, R.A.J. Riddle and D.I. Bonbright, Nucl. Phys. A 172 (1971) 513.
[42] F. Ajzenberg-Selove, Nucl. Phys. A 490 (1988) 1.
[43] J.L. Durand, J. Arvieux, C. Perrin and G. Perrin, Phys. Lett. B 53 (1974) 57.